Fuel 305 (2021) 121424

Contents lists available at ScienceDirect

Fuel

journal homepage: www.elsevier.com/locate/fuel

Modeling the motion of fuel particles in a fluidized bed

A. Köhler [a,*], E. Cano-Pleite [b], A. Soria-Verdugo [b], D. Pallarès [a], F. Johnsson [a]

[a] Dept. of Space, Earth and Environment, Chalmers University of Technology, 412 96 Göteborg, Sweden
[b] Dept. of Thermal Engineering and Fluid Mechanics, University Carlos III of Madrid, 28911 Leganés, Madrid, Spain

ARTICLE INFO

Keywords:
Fluidized bed
Modeling
Fuel mixing
Lateral dispersion
Biomass

ABSTRACT

A semiempirical model for the mixing of fuel particles in a fluidized bed is presented and validated against experimental data from the literature regarding lateral fuel mixing. The model of fuel particle mixing categorizes the fluidized bed into three mixing zones: a rising bubble wake solid zone, an emulsion zone with sinking bulk solids, and a splash zone located above the dense bed. In the emulsion zone, the axial motion of the fuel particle is described by a force balance, applying a viscoplastic stress model, i.e., with a dominant yield stress and only a minor contribution of the shear stress, using an empirical expression from the literature. In the lateral direction, the model is divided into so-called 'recirculation cells', which are crucial for the lateral mixing.

Comparisons of the modeled and measured lateral dispersion coefficients of different fuel types measured in three different large-scale fluidized bed units under both hot and cold conditions (covering a broad range of coefficients: 10^{-4}–10^{-1} m^2/s) reveal satisfactory agreement. The validated model was used to investigate how the lateral mixing of fuel particles depends on the excess gas velocity, the bed height, and the lateral distribution of bubbles over the bed cross-section (which is typically uneven in industrial FB furnaces), as well as the size and density of the fuel particles.

1. Introduction

Fluidized bed (FB) units are applied as industrial chemical reactors due to their ability to convert low-quality solid fuels with high efficiency, while maintaining low levels of emissions. In fluidized bed boilers, the homogeneous and low temperature limits NO_x emissions, while at the same time sorbent bed materials can be used for in-bed capture of SO_x emissions. Fluidized bed combustion entails favorable mixing of the solid fuel and combustion air and high heat and mass transfer rates. Fuel mixing is an important design parameter, determining performance and emission levels [1]. It has been shown that axial fuel mixing influences the mass and heat transfer between the fuel particles and the bed [2], thereby affecting the reactivity of the char particles that result from devolatilization [3], as well as the rate of lateral mixing [4]. In turn, lateral fuel mixing is important for the design of fluidized bed units [5], e.g., to avoid the establishment of high concentrations of volatile matter and char close to the fuel feeding ports [6], which would create undesirable temperature profiles [7] and generate increased levels of emissions [1], especially when fuels with high contents of volatiles, such as biomass, are converted. Understanding the mechanisms behind both axial and lateral mixing, i.e., being able to estimate reliably their rates, would improve the design of fluidized bed reactors so as to facilitate, for example, the minimum number and location of fuel feeding ports [8,9] based on economic criteria [10].

Experimental studies of solids mixing reported in the literature can be divided into two categories: those analyzing the mixing of tracer particles with similar physical properties (density, size) as the bed material; and those investigating the mixing of fuel-like particles, which are typically lighter and larger than the bed solids. For the former studies, Rowe et al. [11,12], who were pioneers in visualizing the mixing of bed solids with x-ray photographs of bubbles rising through gas-fluidized beds, have provided an overview of the important mechanisms underlying axial mixing and the segregation of bed solids in gas-fluidized beds [13]. As for the lateral dispersion of bed solids, Niklasson et al. [10] and Breault [14] have reviewed various studies and correlations for the dispersion coefficients found in the literature. A review of the non-invasive experimental techniques employed to study solids mixing in fluidized beds can be found in the report of Chaouki et al. [15].

Fuel particles, which are typically lighter and larger than the bed solids, are generally assumed to follow the gulf stream pattern established for the bulk solids [16]. The motion of large objects in gas-solids fluidized beds has been the subject of numerous studies in pseudo-2-dimensional (2.5D) beds that allow direct visual tracking [16–22], as

* Corresponding author.
E-mail address: anna.koehler@bioshare.se (A. Köhler).

https://doi.org/10.1016/j.fuel.2021.121424
Received 26 March 2021; Received in revised form 6 July 2021; Accepted 9 July 2021
Available online 3 August 2021

Notation

Roman letters

a	Acceleration, m/s^2
A_0	Bubble catchment area, m^2
C_D	Drag coefficient, –
D	Dispersion coefficient, m^2/s
d	Diameter, m
f_2	Empirical expression, –
f_w	Bubble wake fraction, –
g	Gravitational acceleration, m/s^2
H_0	Fixed bed height, m
L	Recirculation cell length, m
m	Mass of fuel particle, kg
q	Probability to start rising, %
t	Time, s
u	Velocity, m/s
$\dot{V}$	Volumetric flow rate, m^3/s
x	Length, m
Y	Stress effects to gravity effects
z	Axial position, m

Greek letters

α	Fuel-to-bubble velocity ratio, -
δ	Bubble density, -
Δ	Increment, -
θ	Angle, radial displacement, °
ρ	Density, kg/m^3
σ_c	Bubble distribution, -
τ	Shear stress, Pa
φ	Angle, angular displacement, °

Indices

b	Bubble
br	Single bubble
B	Bubble at the bed surface
em	Emulsion
in	Inside the bed
lat	Lateral
mf	Minimum fluidization
o	Initial
out	Outside the bed
p	Fuel particle
s	Bulk solids
tf	Throughflow
tot	Total
vis	Visible
x	x direction
y	y direction

well as in 3-dimensional (3D) beds [23–28] using a large variety of experimental techniques to track solids tracers. These studies have enhanced our understanding of the axial mixing of fuel-like particles, revealing fuel mixing patterns that are strongly coupled to the bubble flow. While all of these studies have been performed in cold laboratory-scale units, the application of Magnetic Particle Tracking (MPT) in a fluid-dynamically downscaled FB by the authors of this work [29,30] has enabled the simulation of the hot large-scale conditions that are prevalent in FBs used for fuel conversion. The latter studies have revealed that parameters important for mixing, namely the particle velocity and the wake volume of the rising bubbles, are underestimated in the literature data derived from non-scaled, cold laboratory-scale experiments [30]. The lateral mixing has been experimentally quantified using a wide range of techniques, including both indirect (through distributions of temperature [5] and gas species [5,7,10,31]) and direct (visual particle tracking [4] and tracer sampling [32,33]) methods.

In addition to the knowledge of the gulf stream patterns of bulk solids and their importance for the mixing of fuel particles [16], Pallarès et al. [34] have shown experimentally that in wider units, several such flow patterns coexist in horizontally aligned arrangements. These flow regions, each established around a preferential bubble path, are called mixing (or recirculation) cells, and they constitute a key concept concerning lateral solids mixing within large beds. Furthermore, Sette et al. [33] have confirmed that the lateral mixing rate of fuel particles can differ significantly from that of the bed material and, thus, it deserves special attention. The larger and lighter fuel particles are more likely to segregate axially and float on top of the bed surface [35–38], depending on the gas velocity and the extension of the splash zone above the dense bed. Such segregation usually enhances lateral mixing, although it still is typically identified as a limiting factor for the performance of large-scale fluidized bed units [31].

Despite its critical importance (especially in large-scale units), there is a lack of modeling tools that can provide reliable descriptions of the fuel mixing. Instead, knowledge of this topic is mainly from the limited amount of experimental data and correlations specific to each fuel, unit and operational condition (see Olsson et al. [4] and references therein). There have indeed been attempts to describe fuel mixing through

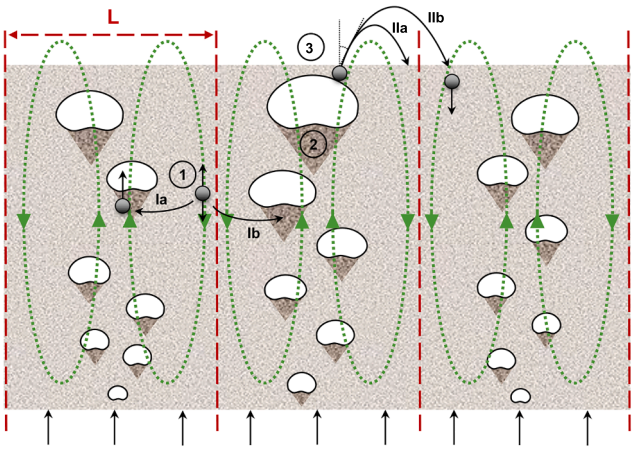

Fig. 1. Schematic of the model of fuel particle motion in the three different zones identified in a fluidized bed. 1) the bubble-free gas-solids emulsion with sinking bulk solids; 2) the bubble wake zone; and 3) the splash zone located above the dense bed. In the lateral direction, the bed is divided into a recirculation cell of length *L*. The interactions with bubbles in the bed may lead to (I) the particle starting to rise in a) the same cell or b) a neighboring cell. On the bed surface, bubble eruption leads to (II) ejection of the particle into a) the same cell or b) any other cell.

computational fluid dynamics (CFD) modeling [39,40], although the methods are still under development (demanding for example multi-grid approaches [41]), and are not yet computationally affordable for large-scale units.

In this work, we propose a model to describe the axial and lateral motions of fuel particles in a fluidized bed (dense bed and splash zone). The model is validated with experimental data on large-scale units available in the literature, i.e., for three different industrial fluidized beds operated under bubbling conditions [4,10,32]. After validation, the model is used to analyze how the lateral mixing of fuel particles depends on the excess gas velocity, the bed height, and the lateral distribution of

bubbles over the bed cross-section (which is typically uneven in industrial FB furnaces). The work has been carried out in collaboration with a major boiler manufacturer, in which a holistic semiempirical model of FB combustion, including fuel mixing, is used for design purposes of industrial FB applications.

2. Theory

Fig. 1 show the basic schemes for the movement of fuel particles and their interactions with bubbles and bed solids, divided into three zones (indicated with Arabic numerals). Inside the dense bed there is: (1) a bubble-free gas-solids emulsion zone with sinking bed solids dragging the fuel particles; and (2) a bubble wake zone that consists of gas bubbles and bed solids that are dragged upwards in the bubble wake, eventually entraining the fuel particles. In the splash zone above the bed surface (3), a ballistic motion is induced by erupting bubbles, leading to lateral scattering of the bed solids and fuel particles.

In the lateral direction, recirculation cells of length L are aligned, with each one established around one bubble path. The mechanisms for lateral displacement are indicated by Roman numerals. Inside the bed, the fuel particles may be trapped by passing bubbles and join the rising bubble flow (I) of either the same cell (Ia) or the closest neighboring cell (Ib), while particles ejected by bubble eruptions at the dense bed surface (II) may end up falling back into the same cell (IIa) or into a neighboring cell (IIb). Note that the change of mixing cell contributes to the effective macroscopic mixing in the lateral direction, while circulation within the same mixing cell yields no such phenomenon.

With the gas bubbles being the main driving force for the mixing of solids in FB units, the formulation of the model starts with a description of the bubble flow, deriving the bubble rise velocity, u_b, and the volume fraction of the bubble phase, δ, as given below.

2.1. Bubble and bulk solids flows

The total volumetric gas flow rate supplied to the bed, $\dot{V}_o$, can be divided into three phases, each characterized by a superficial gas velocity: i) a gas flow at minimum fluidization velocity, $\dot{V}_{mf}$, which holds the gas-solids emulsion at the minimum fluidization level; ii) a gas flow, $\dot{V}_{vis}$, which rises as visible bubbles through the bed [42,43]; and iii) a so-called gas 'throughflow' in and between the bubbles, $\dot{V}_{tf}$, [44,45], which is particularly significant at high gas velocities, such as those used in industrial large-scale FB units, as shown by Johnsson et al. [46]:

$$\dot{V}_o = \dot{V}_{mf} + \dot{V}_{vis} + \dot{V}_{tf} \tag{1}$$

Note that the use of a division of the gas in terms of volumetric flow implies that in-bed variations in pressure, temperature or molar flow will yield a less accurate description of the gas flow. For the specific case of large-scale solid fuel combustion, and based on standard operation data from several authors [47,48], the absolute pressure decreases around 5% (for a bed operating at atmospheric pressure level and with height of 0.5 m) along the bed height, the variations of the measured temperature over the dense bed are around 0.5% [47], and the gas molar flow increases by roughly 2% due to char oxidation partially yielding CO instead of CO_2 (classical gas compositions can be found here [48]). All these facts represent deviations from the assumption of a constant volumetric gas flow expressed by Eq. (1) and the expressions below derived from this equation. Thus, rather than an exact closure of the mass balance of the gas phase, the present work makes use of an approximation which simplifies the modeling. It should also be pointed out that the time averaged pressure drop is constant up through the bed (in cold beds as well as in hot beds with combustion [46]) which indicate that the total time averaged volumetric gas flow is constant.

Each of the components of Eq. (1) can be expressed per unit area of the bed, allowing them to be handled in terms of a corresponding gas velocity. In addition, the visible bubble flow can be expressed as the product of the cross section occupied by bubbles (represented by the void fraction occupied by the bubbles, δ, and called *bubble density*) and the local bubbles rise velocity, u_b, so that the total gas flow into the bed reads:

$$u_o = u_{mf} + u_{vis} + u_{tf} = u_{mf} + \delta u_b + u_{tf} \tag{2}$$

In its turn, the bubble rise velocity can be written as the sum of the velocities for the visible bubble flow and a single rising bubble, u_{br}, which can be expressed as a function of the bubble diameter, d_b, using the correlation of Davidson and Harrison [42]:

$$u_b = u_o - u_{mf} - u_{tf} + u_{br} = u_o - u_{mf} - u_{tf} + 0.711\sqrt{g d_b} \tag{3}$$

Furthermore, the bubble diameter, d_b, is assumed to follow the well-known correlation of Darton et al. [49]:

$$d_b = 0.54 g^{-0.2}\left(u_o - u_{mf}\right)^{0.4}\left(z + 4\sqrt{A_0}\right)^{0.8} \tag{4}$$

where z is the vertical location of the bubble and A_o is the bubble catchment area characterized by the spacing between gas-distributing nozzles.

The bubble density can be obtained by combining Eqs. (1) and (2), yielding:

$$\delta = \frac{1}{1 + \frac{u_{br}}{u_o - u_{mf} - u_{tf}}} \tag{5}$$

An expression for the throughflow is given by Johnsson et al. [46], using Eq. (4) on the basis of a constant pressure gradient over the bed height, i.e., resulting in a constant bubble density with dense bed height:

$$u_{tf} = \left(1 - f_2\left(z + 4\sqrt{A_o}\right)^{0.4}\right)\left(u_o - u_{mf}\right) \tag{6}$$

where f_2 is an empirical expression that they derived from their experiments in a large-scale hot bubbling fluidized bed, using sand as the bed material:

$$f_2 = [0.26 + 0.70 exp(-0.0033 d_s)]\left[0.15 + \left(u_o - u_{mf}\right)\right]^{-0.33} \tag{7}$$

where d_s is the average diameter of the bed solids.

In the emulsion zone, the bed solids are sinking to make up for the solids that are being dragged up by the rising bubbles. Combining the above expressions for the bubble flow (i.e., for δ and u_b) with the wake volume fraction of the bubbles, f_w, as given by Kunii and Levenspiel [50], a mass balance over the bed solids in a horizontal bed slice can be formulated. This results in the velocity of the sinking bulk solids in the emulsion zone being expressed as:

$$u_{s\downarrow} = \frac{f_w \delta u_b}{(1 - \delta - f_w \delta)} \tag{8}$$

Values for the wake volume fraction are obtained from cold laboratory-scale experiments using Geldart B particles of various sizes and densities, according to Rowe et al. [11]. However, the values appear to underestimate conditions that are valid for hot industrial-scale units. Thus, a higher value of 0.63 is used here, which was found by fitting the axial model with the minimum square error [51].

2.1.1. Lateral distribution of bubbles

The pressure drop through the air distributor plate affects the distribution of bubbles throughout the bed cross-section. According to Karri and Werther [52], a relatively high pressure drop across the air distributor is required to guarantee an even lateral distribution of the bubbles and homogeneous fluidization. In contrast, the requirement for low power consumption means that FB boilers must employ gas distributors with a relatively low pressure drop [1], leading to large bubbles that may be unevenly distributed over the bed cross-section. Given a sufficiently large cross-section, the formation of toroidal solids flow

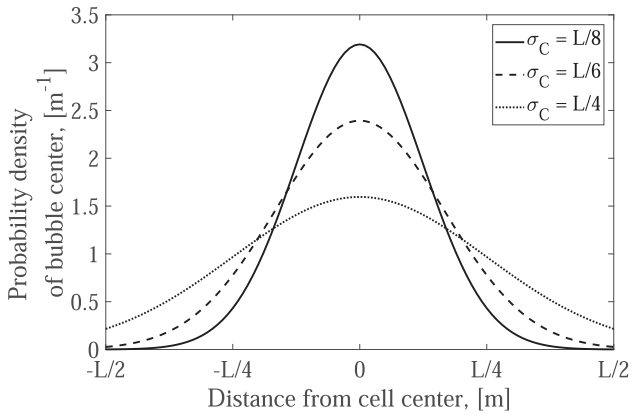

Fig. 2. Probability Density Function (PDF) of the assumed lateral distributions of the bubble eruptions within a recirculation cell.

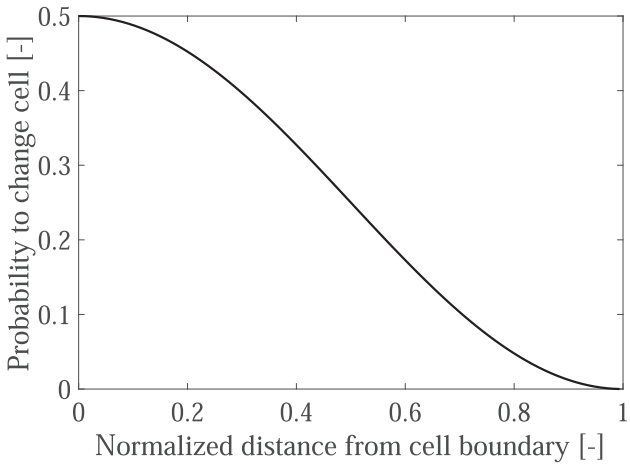

Fig. 3. Probability of a tracked particle changing recirculation cell inside the dense bed.

structures around preferred bubble paths will create recirculation cells, with solids being drawn up by the rising bubbles and descending in-between the bubble paths [4,34]. There are reports in the literature that have evaluated the solids and gas velocity in the recirculation cells inside the bed by solving the averaged dynamic equations of the flow [51,52]. However, this type of approach dramatically increases the complexity of the model. Furthermore, while no simple models are available in the literature to determine the sizes of these recirculation cells, an estimation can be made based on the proposal of Abanades and Grasa [53], using the ratio of the bed dimension to the bubble diameter at the bed surface, d_B, thereby deriving a recirculation cell length of $L \sim d_B$.

Regarding the internal lateral distribution of the bubbles within a specific recirculation cell (i.e., how dominant the main bubble path is), Whitehead [53] carried out experiments in a sand bed with cross-sections ranging up to 2.44 × 2.44 m^2 fluidized by air under ambient conditions by means of tuyere nozzles with similar spacing to that used in the industrial units from which the validation data for this work are taken [4,10,32]. The horizontal distribution of bubble eruptions over the surfaces of different units, under different operational conditions, and with different gas distributors, were studied, to identify significant variations that depended on these parameters. In the model, these variations are represented by a normal lateral bubble distribution centered on the middle of the recirculation cell (where the preferential path for the bubble is located) and with a standard deviation, σ_C. From the graphical data of Whitehead [53], which specified the locations of several individual bubble eruptions, a value of $\sigma_C = L/6.9$ was obtained and introduced as an input parameter to the model. Furthermore, the effect of σ_C was studied considering the following three different standard deviations: *L/8, L/6,* and *L/4*, where *L* is the recirculation cell size. Fig. 2 gives the Probability Density Function (PDF) of the assumed centers of bubble eruptions along the length of a recirculation cell when applying these standard deviations.

2.2. Fuel mixing

The motion of the fuel particle is here assumed to be governed by the solids flow and the two mechanisms (I and II) associated with the three zones (1: emulsion; 2: bubble wake; 3: splash zone), as indicated in Fig. 1. Below, the expressions governing the mixing of a fuel particle in each of these three zones are presented.

2.2.1. Fuel in the emulsion zone

The acceleration of the fuel particle in the emulsion zone is calculated using the equation of motion from the sum of the forces acting on the fuel particle, where the drag force from the bed uses the sinking bulk solids velocity (*cf.* Eq. (7)), reading:

$$a_p = \left(\frac{\rho_{em}}{\rho_p} - 1\right) g + \frac{3}{4}\frac{\rho_{em}}{\rho_p}\frac{C_D}{d_p}\left|\left(u_{s\downarrow} - u_p\right)\right|\left(u_{s\downarrow} - u_p\right) \tag{9}$$

The drag coefficient from the bed acting on the fuel particle, C_D, can be obtained from a recent work conducted by the authors (Köhler et al. 2021), in which the bed emulsion was shown to exhibit a viscoplastic rheology acting on immersed particles with a dominant yield stress and only a slight contribution of the shear stress for typical shear rates (up to 5 s^{-1}). A way to study the rheology of viscoplastics is to compare the stress effects with the gravity effects [54]. With this, the shear stress of the bed emulsion on the tracked particle can be expressed as a function of the particle diameter and relative density and is fitted to:

$$Y = \frac{\tau}{g d_p\left(\rho_{em} - \rho_p\right)} = 0.167 + 0.042\left(\frac{u_{s\downarrow} - u_p}{d_p}\right)^{0.336} \tag{10}$$

From the shear stress, τ, the drag coefficient is expressed as:

$$C_D = \frac{8\tau}{\rho_{em}\left(\left|u_{s\downarrow} - u_p\right|\right)^2} \tag{11}$$

2.2.2. Fuel in the bubble wake zone

The fuel particle enters the bubble wake zone when it is caught by passing bubbles, which occurs with a probability q for each bubble passage. As discussed in the previous presentation of the model for fuel axial mixing [51], this probability is somewhat dependent upon the axial position and the fluidization velocity, although using a constant value of 0.21 yielded modeled fuel distributions that were in good agreement with the measurement data [51].

Whether the tracked particle joins a bubble path within the same recirculation cell or in the closest neighboring cell is described through the sinusoidal probability curve shown in Fig. 3: at the cell boundary there is a 50% probability to change cell, while at the mixing cell center the probability is zero.

To determine the new position of the particle after lateral displacement, an angular position through the angle φ and a radial position through the angle θ are assigned (*cf.* Fig. 4). These angles are also used in the splash zone and are explained in the corresponding section.

Moreover, the probability for a tracked particle to leave the bubble wake zone has been shown to be low, and it plays a minor role in the description of the axial fuel particle mixing model [51]. Thus, once the fuel particle has entered the bubble wake zone, it is assumed to ascend in the bed by alternately joining and detaching from different wake regions until it reaches the dense bed surface. This results in an axial displacement at an average velocity, which can be expressed as a fraction of the bubble velocity:

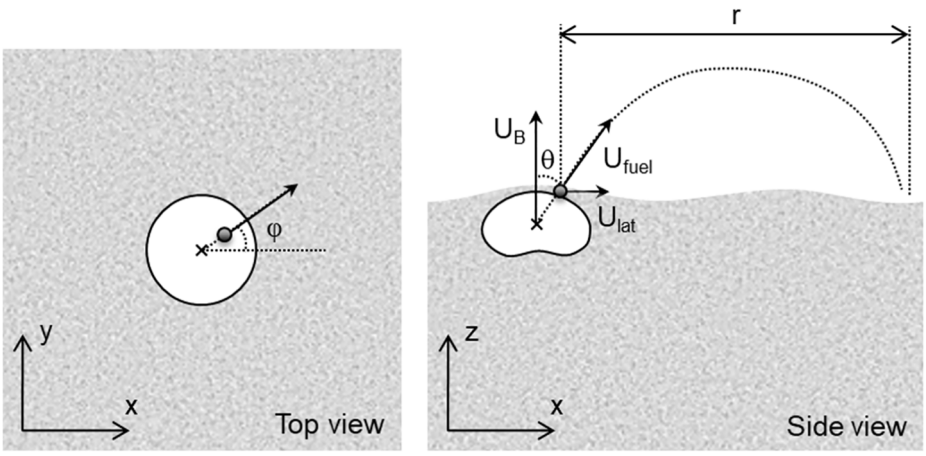

Fig. 4. Particle ejection angles assigned for lateral displacement.

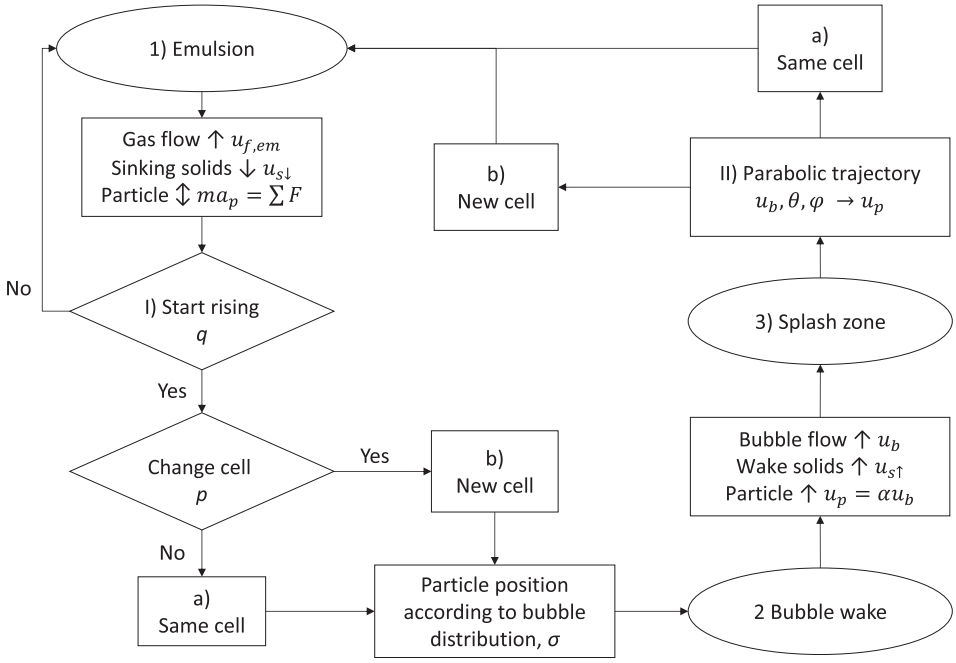

Fig. 5. Computational flow diagram of the model used for fuel particle tracking.

$$u_p = \alpha u_b \tag{12}$$

The values of α reported in the literature range from 10% to 30% [16,17,19,35,55], representing data obtained from experiments with a wide variety of units, materials, and operational conditions. However, as seen in a previous work by the authors [30], the use of conditions relevant to hot industrial units results in much higher values of α. Here, a value of 0.6 is used for α, which was shown previously to work well as a benchmark for the axial model [51].

2.2.3. Fuel in the splash zone

When it reaches the dense bed surface, the fuel particle is ejected into the freeboard by the erupting bubble. Experimental findings show that the motion of a fuel particle induced by the bubble eruptions follows a parabolic path [56]. The modulus of the ejection velocity of the fuel particle, u_p, is a function of the bubble velocity, u_b, and the ejection angle, θ, (see Fig. 4):

$$u_p = u_b|_{z=H_0}\cos(\theta) \tag{13}$$

The ejection angle, θ, follows a probability given by the same experiments as:

$$P(\theta) = 0.046\exp(-0.045\theta) \tag{14}$$

Furthermore, the model includes a scatter of the bubble velocity in the form of a coefficient that follows a Gaussian distribution with a mean of 1 and a standard deviation of 0.32, as described previously [56].

As for the lateral movement inside the bed, the azimuthal direction followed by the fuel particle is delineated, using the uniformly distributed angle φ, with the line connecting the bubble center and the particle location at the time of ejection. With the vertical component of the ejection velocity and the gravity as the sole force, the particle is assumed to follow a ballistic trajectory. Once the fuel particle completes its trajectory in the freeboard and lands on the bed surface, it is immersed back into the emulsion zone.

3. Implementation of the model and determination of dispersion coefficients

The present work models fuel mixing by continuously tracking the fate of a single fuel particle, following the flow diagram in Fig. 5, with its

Table 1
Input parameters taken from the literature and applied in the model validation cases.

Variable	Qian et al. (1987) [32]	Niklasson et al. (2002) [10]	Olsson et al. (2012) [4]
Bed cross-section, m^2	2.6 × 1.6 = 4.16	1.7 × 1.7 = 2.89	1.7 × 0.85 = 1.44
Bubble catchment area, m^2	0.0201	0.0201	0.0241
Bed material particle density, kg/m^3	2,600	2,600	2,600
Bed material particle size, μm	1,420	700	150
Temperature	Ambient temperature	900 °C	Ambient temperature
Minimum fluidization velocity, m/s	0.63	0.17	0.02
Bed height, m	0.25; 0.30;0.35	0.5	0.4
Gas velocities, m/s	0.68; 0.75; 0.86; 1.03	2.30	0.10; 0.15
Fuel	Continuous feed of spherical bituminous coal	Continuous feed of wood chips (moisture content, 45%)	Batch of 7 × 15 bark pellets
Fuel density, kg/m^3	1,340	810	1,180
Fuel particle size, expressed as equivalent diameter, mm	14.0	37.0	12.8

motion governed by the expressions given in Section 2 for the three different fluid dynamic zones illustrated in Fig. 1. The particle trajectory is tracked with time-steps of $5e^{-3}$ s for a given simulation time, and the modeled trajectory data generated are used to extract the lateral dispersion coefficients. Note that tracking only a single particle with constant size and density implies that interactions between different fuel particles are not considered in the model.

The model follows the flow diagram given in Fig. 5, assuming the following: the fuel particle (through over bed feeding) initially falls on the dense bed surface, and it is immersed into the bed (emulsion zone), where only axial displacement takes place. Eventually, the particle is caught by a passing bubble and enters the bubble wake zone, where it follows the rising motion of the bubble. Entrapment by a passing bubble induces a lateral displacement, which may or may not represent a change in the mixing cell. When it reaches the bed surface, the particle is ejected into the splash zone, where it follows a ballistic trajectory, eventually landing back onto the dense bed surface, in the same or a different mixing cell, and starts to become immersed once again in the emulsion zone. Note that neither variations in particle size/density due to chemical reactions nor effects of attrition or particle entrainment were considered in the model, for the sake of simplicity. Nonetheless, the model could be extended by assuming the evolution of particle size/density during the fuel conversion and/or including sub-models that consider the influences of attrition and particle entrainment on the fuel motion.

The input parameters to the model are the geometry of the reactor, the operating conditions (bed height, fluidization velocity, and properties of the solids phase) and the lateral distribution of erupting bubbles in the bed cross-section.

At a macroscopic level, i.e. at a length scale larger than that of the recirculation cells originated by the toroidal solids flow structures introduced in *Theory*, the lateral mixing of fuel in the bed and splash zone of FB units can be approached as a stochastic process characterized by a lateral dispersion coefficient, $D_{x,y}$. Once sufficient trajectory data are generated by the tracking model, this coefficient can be calculated from Einstein's equation [57]:

$$D_{x,y} = \frac{\left(\Delta_{x,y}\right)^2}{2\Delta t} \tag{15}$$

This work considers quadratic recirculation cells (equal nozzle spacing in the x- and y-directions) resulting in isotropic mixing of the fuel particles in the lateral directions, i.e., $D_x = D_y = D_{lat}$.

In order to illustrate the statistical representability of the modeled data, the input data from Qian et al. [32] have been used (*cf.* Table 1) to simulate 15-min-long trajectories of a fuel particle. The final location of the particle in each simulation provides a value for the lateral dispersion coefficient according to Eq. (14), summing to a distribution of dispersion coefficient values. Since, as discussed above, the lateral motion of fuel particles in a bubbling fluidized bed at a macroscopic scale larger than that of the recirculation cells can be seen as a stochastic process, the

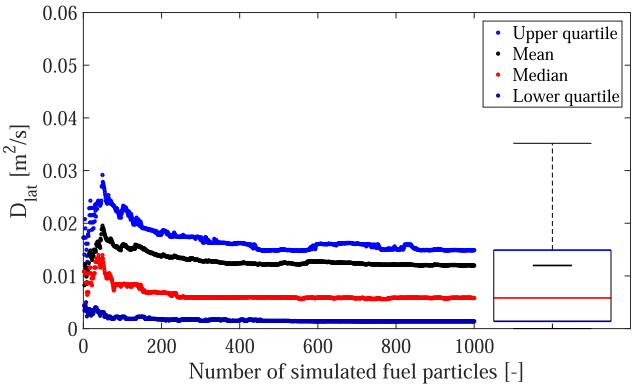

Fig. 6. Effects of the number of fuel particles included in the simulation of the lateral dispersion coefficients. Modeling case: Qian et al. [32].

lateral dispersion coefficient values obtained from the trajectories of each particle follows a statistical distribution. Fig. 6 shows the evolution of some of the statistical parameters for this distribution, namely the mean, the median, and the upper and lower quartiles, of the distribution of lateral dispersion coefficients obtained when varying the number of simulated trajectories of a single fuel particle. A boxplot of the lateral dispersion coefficient for the simulation of the motion of 1,000 trajectories is also included in Fig. 6. In a boxplot, the entire statistical distribution is shown in a compact way, representing a box that is bounded by the lower and upper quartiles, i.e., the values higher than 25% and 75% of the data in the distribution, respectively. The line in the middle of the box represents the median, which is the value higher than 50% of the data in the distribution. The boxplots include also confidence intervals for the data, represented by dashed lines (called 'whiskers'), which are calculated as the last data-point of the distribution found at a maximum distance of 1.5-times the interquartile distance from the upper or lower quartile. Any data outside these confidence intervals are designated as 'outliers', i.e., data-points with a low probability of occurrence, and they would ordinarily be represented as singular points in the boxplots. However, outliers are not represented here, for the sake of simplicity. In view of the statistical data on the distribution of lateral dispersion coefficients and the boxplot shown in Fig. 6, the statistical distribution is non-normal, as different values are obtained for the mean and the median and the boxplot is not symmetric with respect to the median. Therefore, instead of the mean and the standard deviation, which are the representative values for a normal distribution, the median and the quartiles will be used as representative values for the non-normal distribution of the lateral dispersion coefficients. This information will be reported in the form of boxplots, where the representative values of the distribution are included.

As shown in Fig. 6, the distribution of the lateral dispersion

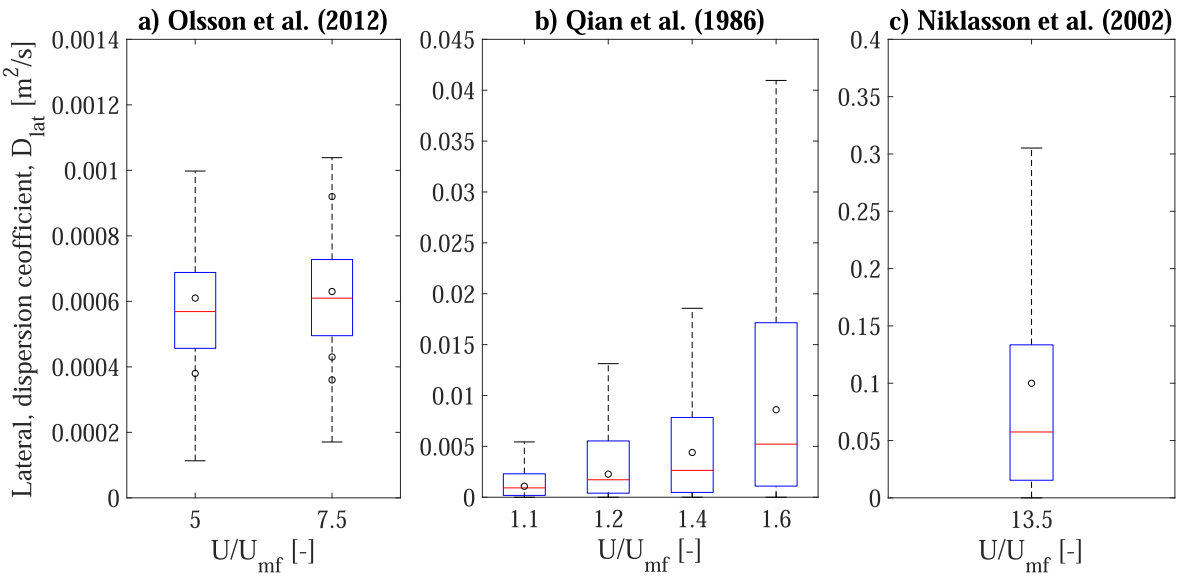

Fig. 7. Boxplots for the model validation comparing the experimentally derived values (○) and modeled values of the lateral dispersion coefficient for the three different experimental campaigns reported in the literature: a) Olsson et al. [4]; b) Qian et al. [32]; and c) Niklasson et al. [10]. Note the different scales on the *y*-axes.

coefficient becomes relatively stable when one considers approximately 500 simulations and is highly reliable when one examines>700 simulations.

Finally, note that while statistical robustness is attainable in the evaluation of the modeled lateral dispersion coefficient, experimental data face the challenge of dealing with finite geometries, and this often limits the ability to extract statistically robust experimental values. Therefore, it is not certain how robust the experimental values reported in literature are, since they are derived from finite geometries and for a limited number of fuel particles.

4. Results and discussion

This section starts by validating the model against experimental data from large-scale studies in the literature. Thereafter, the model is used to study the sensitivity of fuel mixing for different parameters.

4.1. Model validation

Three different experimental large-scale campaigns, found in the literature [4,10,32] and summarized in Table 1, are used to validate the model [Eqs. (1)-(13)] in terms of the lateral fuel dispersion.

Qian et al. [32] conducted cold experiments in a rectangular boiler of 4.16 m^2 and obtained the lateral dispersion of continuously fed spherical bituminous coal particles. The temperature is not given but is assumed to be according to ambient conditions. To obtain the lateral dispersion coefficient, they measured the fuel concentration by collecting the fuel particles from 15 compartments of a grid over the bed during several rounds. After the first round, fuel feeding was stopped and the procedure was continued until all the tracer particles were distributed evenly over the bed. Since the arrangement of the nozzles is not reported, it is here assumed that the nozzles have the same bubble catchment area of 0.0201 m^2 as given by Niklasson et al. [10] for a typical industrial-scale boiler.

Niklasson et al. [10] measured the lateral fuel dispersion at a temperature of 900 °C in a square boiler of 2.89 m^2 using a grid of moisture sensors over the bed to derive the concentrations of continuously fed wet wood chips as they spread over the bed. The fuel density is not given but is estimated to be around 810 kg/m^3. The fuel particle size is given as a log-normal distribution of the surface area divided by the volume (with a mean of 710 m^{-1}). As the model handles only spherical tracers, these wood chips are in the present work approached using a sphere that yields the same projected area as standard wood chips (taken as 0.001 m^2 [4]), resulting in a diameter of 0. 37 m.

Olsson et al. [4] carried out measurements of the lateral dispersion coefficient in a bubbling fluidized bed that had a rectangular cross-sectional area of 1.44 m^2. They applied ambient air as the fluidizing gas with fluidization velocities of 0.10 m/s and 0.15 m/s. Using seven repetitions of a batch test with 15–20 bark pellets particles in each, the lateral dispersion coefficient was measured by digital image tracking of the individual particles, which were labeled with small phosphorescent plastic capsules. They limited the experimental time to 6 min and 30 s and calculated the final lateral dispersion coefficient by averaging the dispersion coefficient over a period of 5 min. If a particle reached the opposite wall earlier, the average was taken from the reduced time period. Note that they used cylindrical particles (21 × 8 mm), for which the equivalent diameter of 12.8 mm is a reasonable approximation.

Note that the modeled values of the dispersion coefficient in Fig. 7 are represented as a statistical distribution, as obtained from each respective series of individual particle simulations. In this work, 1,000 fuel particles were modeled for the validation study with the cases shown in Table 1, which ensured the statistical robustness of the extracted values for the lateral dispersion coefficients. It should be noted that the experimental values reported by Olsson et al. [4] were extracted from seven runs with a batch of 15 fuel particles in each. To resemble fully the experiments, the model simulates 1,000 batches of 15 particles and the simulation was stopped once the first particle of each batch reached the wall.

Fig. 7 compares the experimentally derived values (indicated with ○) and modeled values of the lateral dispersion coefficient for the three different large-scale set-ups reported in the literature: a) Olsson et al. [4]; b) Qian et al. [32]; and c) Niklasson et al. [10], as presented in Table 1. It is clear that most of the experimental values lie within the quartiles of the distribution, i.e., within the 25% and 75% percentiles, represented in the boxplots derived from the 1,000 modeled trajectories for each case. In fact, only some of the experimental results from Olsson et al. [4] present values that lie outside the quartiles of the dispersion coefficient distribution. However, despite the relatively broad dispersion of these experimental values, they lie within the confidence interval of the distribution represented by the whiskers of the boxplot. It must be emphasized here that the model is capable of representing a wide range of experimental values for the dispersion coefficients (spanning three

Table 2
Input parameters defining the reference case.

Parameter	Model
Bubble catchment area, m^2	0.0201
Temperature, °C	800
Bed material density, kg/m^3	2,600
Bed material size, μm	600
Minimum fluidization, m/s	0.17 m/s
Bed height, m	0.5 m
Excess velocity, m/s	0.86 m/s
Fuel particle volume, m^3	3.6×10^{-5}
Fuel particle density, kg/m^3	810
Number of particles, -	1,000
Time-step, s	5×10^{-3}
Total modeling time, s	15×60

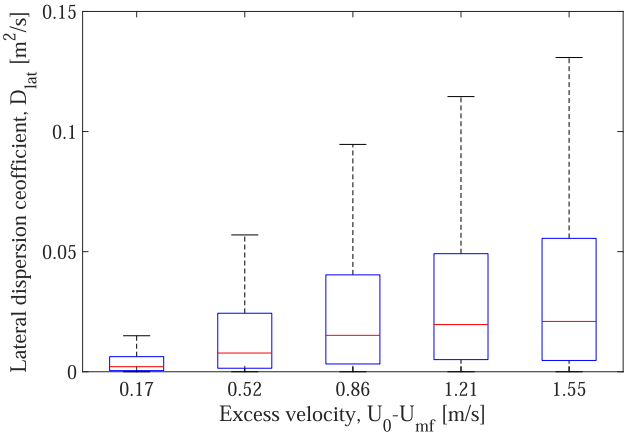

Fig. 8. Effects of the excess velocity, u_0-u_{mf}, on the lateral dispersion coefficient ($H_0 = 0.5$ m, $\sigma_C = L/6.9$).

orders of magnitude), with fluidization numbers in the range of 1.1–13.5. The model is also able to follow the trend of increased lateral dispersion with an increase in fluidization velocity, as shown in Fig. 7b. Thus, while the model presented is semiempirical and includes approximations, it is able to satisfactorily reproduce the measurement data from industrial units available in literature, despite their wide range in operational conditions and measured rates of fuel mixing.

4.2. Sensitivity analysis

This section investigates the influences of different operational conditions (excess gas velocity, bed height), fuel properties (particle density, particle size), and lateral distributions of bubbles in the recirculation cell on the resulting fuel mixing as predicted by the validated model, so as to identify key parameters. For the analysis, a reference case is defined as presented in Table 2. As reference, fuel wood chips are used, while two other typical biomass fuels (bark pellets and dried wood chips) are also considered.

4.2.1. Influence of the lateral distribution of bubbles

Using the input parameters for the reference case, three different bubble distributions, corresponding to σ_c values of $L/8$, $L/6$, and $L/4$, are modeled. The bubble distribution was found to have only a weak influence on the lateral dispersion coefficient, which increased only 7%–15% as σ_c was doubled. Note that in the model formulation, the bubble distribution will influence the lateral mixing but not the axial mixing. In addition, the probability of a fuel particle immersed in the emulsion being trapped by a passing bubble (expressed by q) was obtained from measurements and, thus, already implicitly includes the bubble distribution in the experiments and is not varied by varying σ_C.

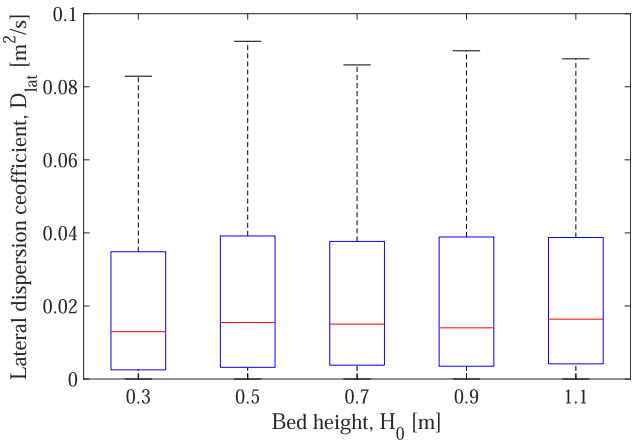

Fig. 9. Effects of bed height on the statistical distribution of the modeled lateral dispersion coefficients (u_0-$u_{mf} = 0.86$ m/s, $\sigma_C = L/6.9$).

4.2.2. Influence of excess gas velocity

Fig. 8 shows that an increase in excess gas velocity promotes an increase of the lateral mixing of the fuel, which is expected considering that the sizes of the recirculation cells increase for higher values of the excess velocity. The results are in line with previous findings for fuel dispersion [9,33] and similar to the results for dispersion of the bulk material [5]. It can also be seen in Fig. 8 that a higher fluidization velocity leads to a broadening of the statistical distribution of the dispersion coefficients. In fact, both enhancement of the lateral mixing of the fuel and broadening of the statistical distribution of the dispersion coefficients were also observed for the specific conditions described by Qian et al. [32] (see Fig. 7b). It should be kept in mind that high excess gas velocities may decrease the flotsam tendency of the fuel, since larger bubbles induce a more vigorous convective vertical mixing [13], causing fuel particles to circulate throughout the entire bed [19].

Given a dense bed height of 0.5 m, the median value of the lateral dispersion coefficient as a function of the excess gas velocity results in a linear relationship – as reported earlier from the experimental data in the literature [33,58] – that can be expressed as $D_{lat} = 0.015(u_0 - u_{mf})$, yielding a determination coefficient of $R^2 = 0.95$.

4.2.3. Influence of the bed height

As the dense bed height influences the size and velocity of erupting bubbles and, consequently, the size of the recirculation cells, an increase in the dense bed height is expected to enhance the lateral dispersion of fuel particles, primarily if the particles are located in the splash zone. In industrial units, the dense bed height is selected so as to minimize the bed pressure drop (and thus fan power costs) while maintaining stable operation. Fig. 9 shows that the modeled lateral dispersion coefficient remains largely unaffected by increasing dense bed height. Similar results have been reported from experiments on tracer particle mixing in a fluid-dynamically downscaled bed [59], while the lateral dispersion of the bulk material is reported to increase significantly with bed height.

The result shown in Fig. 9 can be understood when studying the relative time spent and distance travelled by the tracer inside the bed and in the splash zone, respectively. Fig. 10a-d shows the median of the time spent and of the distance travelled for increases in the excess velocity or dense bed height. As expected, increasing the velocity results in the fuel particles spending more time in the splash zone (Fig. 10a), due to the fact that the bubble eruptions cause longer ballistic trajectories and this translates to an longer distance travelled in the splash zone (Fig. 10b). On the other hand, increasing the bed height leads to a larger fraction of time spent inside the dense bed (Fig. 10c), which reduces the flotsam behavior of the fuel particles and, consequently, the distance travelled in the splash zone remains essentially constant (*cf.* Fig. 10d), due to fewer but more vigorous ejections.

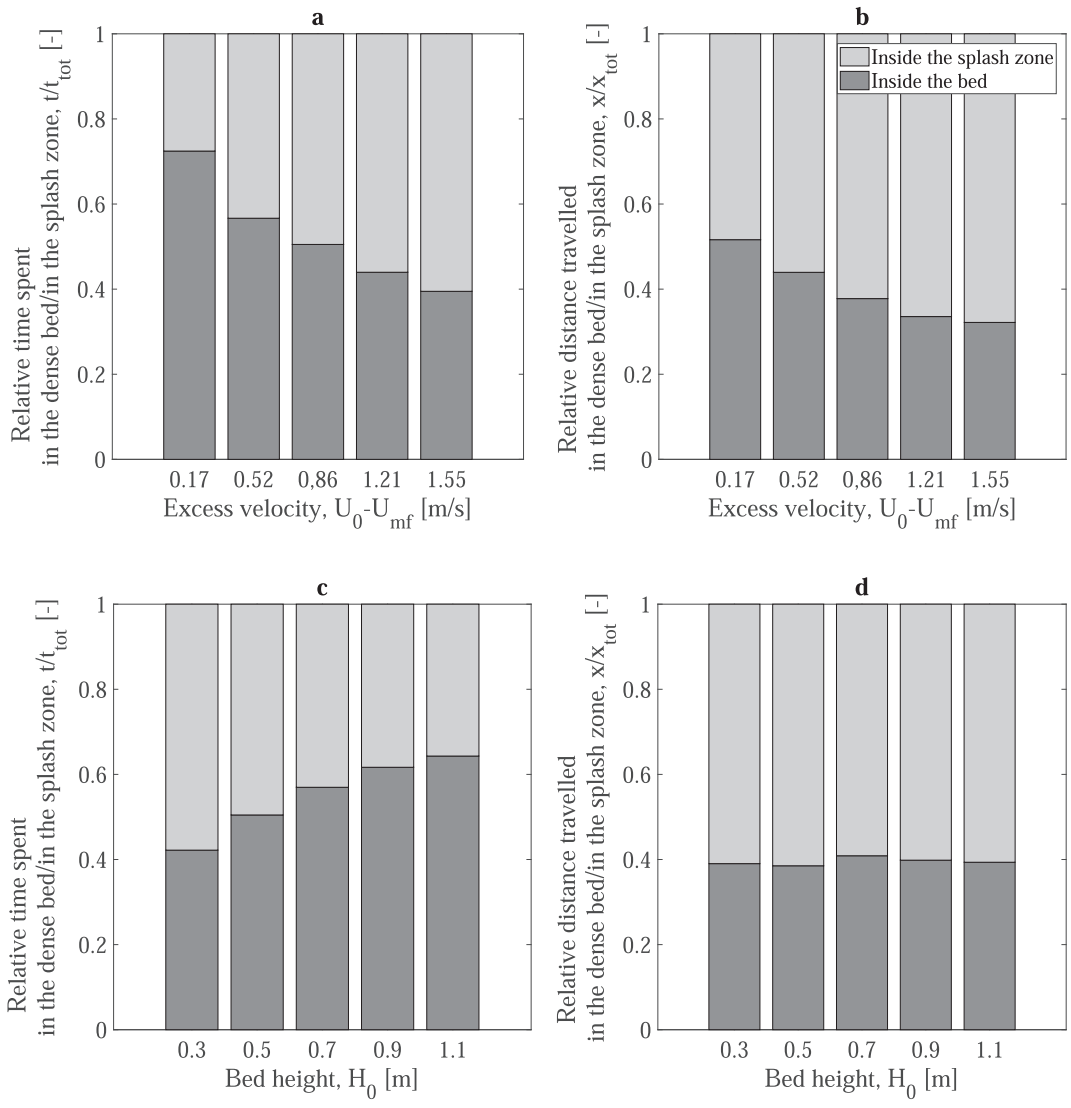

Fig. 10. a) and c) Fractions of time that the fuel particles spent in the dense bed and splash zone, t/t_{tot}. b) and d) Fractions of effective displacement of the fuel particles in the dense bed and splash zone, x/x_{tot}.

Table 3
Lateral dispersion of different fuel particles (density, average diameter).

	Dry wood chips (520 kg/m^3, 4 cm)		Fresh wood chips (810 kg/m^3, 4 cm)		Bark pellets (1,180 kg/m^3, 1.3 cm)	
u_0-u_{mf} [m]	0.17	1.21	0.17	1.21	0.17	1.21
$D_{lat} \times 1000$ [m^2/s]	2.50	19.13	2.12	19.27	2.70	20.47
t_{in}/t_{tot} [–]	0.66	0.44	0.72	0.44	0.65	0.44
t_{out}/t_{tot} [–]	0.34	0.56	0.28	0.56	0.35	0.56
x_{in}/x_{tot} [–]	0.58	0.36	0.54	0.35	0.51	0.34
x_{out}/x_{tot} [–]	0.42	0.64	0.46	0.65	0.49	0.66

These results underline the importance of studying fuel mixing along the entire bed height, which is difficult to achieve experimentally in industrial-scale units.

4.2.4. *Influence of fuel particle properties*

In addition to the reference fuel (wood chips, 810 kg/m^3, 0.04 m), two additional typical biomass fuel types were investigated: dry wood chips (520 kg/m^3, 0.04 m) and bark pellets (1180 kg/m^3, 0.013 m). Table 3 reports the lateral dispersion coefficients for these three fuel types and for two fluidization velocities. Differences in fuel density and size had very weak effects on the lateral dispersion for the fuels studied, with bark pellets exhibiting the largest fraction of time on the bed surface and the highest dispersion coefficient for the low velocity. Increasing the fluidization velocity improved the lateral dispersion by an order of magnitude for all three fuel types, while at the same time the fuel spent more time in the splash zone, where it mixed faster in the lateral direction.

As mentioned earlier, lateral dispersion is higher in the splash zone. As lighter particles are more likely to float on the bed surface, they may promote faster lateral dispersion. Few studies in the literature have compared the mixing of different fuel types (including biomass). However, a study comparing spherical coal particles with heavier washery tailing balls [32] has suggested a slight increase in the dispersion coefficient for lighter and smaller fuel particles. In contrast, a previous work comparing wood chips, wood pellets and the char of wood pellets [59] has reported an increase in the dispersion coefficients for lighter but larger fuel particles. This is in line with the force balance over an immersed fuel particle, which indicates that the net gravitational force (weight-buoyancy, i.e., buoyant for biomass) becomes more dominant for larger particles, as compared to the drag of the sinking bulk solids. Furthermore, it should be noted that the modeling in the present work applies spherical particles of equivalent diameter to the particles used in

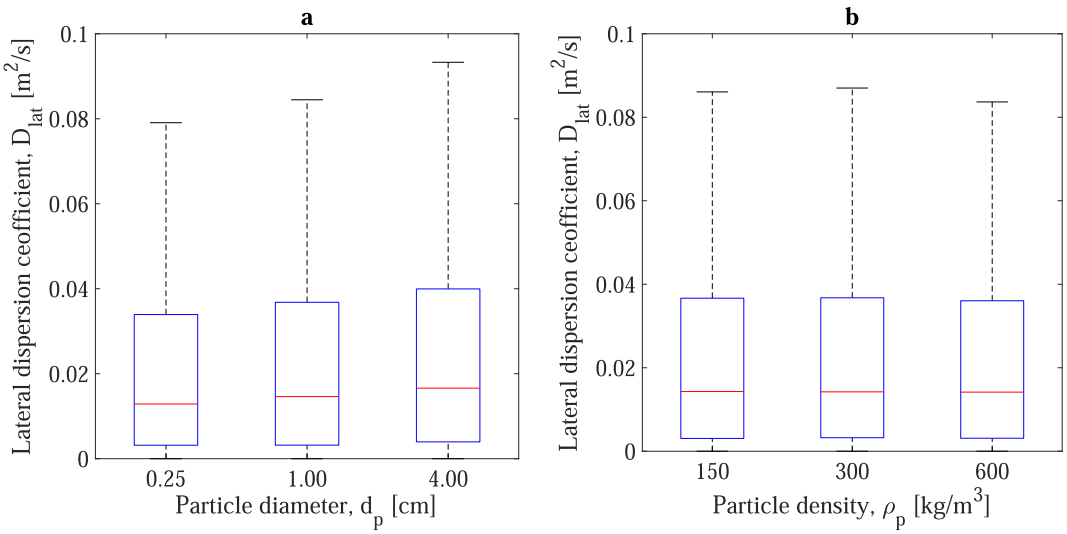

Fig. 11. Effects on the lateral dispersion coefficient (u_0-u_{mf} = *0.86 m/s*, H_0 = *0.5 m*, σ_C = *L/6.9*) of: a) particle diameter, d_p, for a char particle of 300 kg/m^3; and b) particle density, ρ_p, for a char particle of 1 cm.

the experiments (*cf.* Table 1), which might reduce the effect of flotsam behavior and, therefore, the impact on the lateral dispersion.

Due to the long conversion times of char, i.e., >20 min in combustion and > 30 min in gasification [3], a major fraction of the fuel present in the bed is expected to be char. During char conversion under combustion conditions, the particle is assumed to be primarily changing in size (shrinking sphere scheme). Typically for gasification conditions, the particle can be modeled as primarily changing in density (shrinking core scheme). Therefore, although the model does not simulate the ongoing conversion of the fuel, the effects of the different conversion schemes on the fuel motion (namely size or density changes) can be investigated by simulating three different char particle sizes and three different densities and studying their effects on the lateral dispersion of the fuel.

The resulting effects on the lateral dispersion coefficient are shown in Fig. 11 for: a) a varying particle diameter; and b) a varying particle density. A four-fold increase in diameter results in a 12% increase in lateral dispersion, while the distribution becomes slightly broader. This is due to the increased time that the fuel spends in the splash zone, given that its flotsam behavior increases with a larger diameter. Doubling the particle density has a negligible effect on the lateral dispersion coefficient (<1%) for the range investigated. For typical density values of char (150–300 kg/m^3), the particle is spending about 50% of its time in the splash zone, corresponding to 60% of the distance travelled.

5. Conclusions

A model that describes the motions of fuel particles in the bed and splash zone of a fluidized bed was developed and used to evaluate lateral dispersion of fuels in industrial-scale reactors. The model shows good agreement with data from the literature regarding the strongly variable (range, 10^{-4}–10^{-1} m^2/s) lateral mixing of different fuel types measured in three different large-scale fluidized bed units under both hot and cold conditions. The validated model was used to investigate how the lateral mixing of fuel particles depends on the excess gas velocity, the bed height, and the lateral distribution of bubbles over the bed cross-section (which is typically uneven in industrial FB furnaces), as well as the properties of the fuel (size and density).

The model shows that the lateral distribution of bubbles has a minor impact on the lateral dispersion of the fuel particles. Although increasing the bed height results in larger bubbles being present in the bed, there is little effect on the lateral dispersion coefficient in the model, owing to the fact that the time that the fuel spends in the dense bed, where lateral distribution is slower, is increased significantly. This contrasts with the effect of bed height on the lateral distribution of bulk solids.

Increasing the fluidization velocity enhances the lateral dispersion. In relation to the time that the fuel particle spends inside the dense bed, the model results reveal a major decrease with increasing velocity, resulting in a stronger contribution of the lateral dispersion on the bed surface.

For three typical biomass fuel types (dry wood chips, fresh wood chips and bark pellets) at a high and a low velocity, the fuel size and density have weak effects on the share of time and displacement inside the bed, i.e., showing only minor effects on the lateral fuel dispersion. At low velocities, the heaviest and smallest fuel particles spend most of the time on the bed surface, while increasing the velocity improves the lateral mixing equally for all three fuel types.

This work also studied the effects of the size and density of a char particle under typical conversion conditions (combustion or gasification) on the motion of the fuel. It is shown that char particle size has a weak influence, while changing the density of the char particle has no effect on its lateral dispersion.

CRediT authorship contribution statement

A. Köhler: Conceptualization, Methodology, Software, Validation, Formal analysis, Investigation, Writing - original draft. **E. Cano-Pleite:** Methodology, Software, Writing - review & editing, Funding acquisition. **A. Soria-Verdugo:** Conceptualization, Methodology, Validation, Writing - review & editing, Supervision. **D. Pallarès:** Writing - review & editing, Supervision, Project administration, Funding acquisition. **F. Johnsson:** Writing - review & editing, Supervision.

Declaration of Competing Interest

The authors declare that they have no known competing financial interests or personal relationships that could have appeared to influence the work reported in this paper.

Acknowledgments

This work was financed in part by the Swedish Gasification Centre (SFC) within the framework of the Centre for Indirect Gasification of Biomass (CIGB), and by the Swedish Energy Agency within the framework of project P-38347-2. This work was funded in part (receiver E. Cano-Pleite) by the CONEX-Plus program by Universidad Carlos III de Madrid, the European Union's Horizon 2020 research and innovation

program under the Marie Sklodowska-Curie grant agreement No. 801538 and from Programa de Atracción de Talento (Modalidad 2) de la Comunidad de Madrid (Spain), with number 2019-T2/AMB-15938.

References

[1] Leckner B. Fluidized bed combustion: Mixing and pollutant limitation. Prog Energy Combust Sci 1998;24:31–61. https://doi.org/10.1016/S0360-1285(97)00021-X.

[2] Qin K, Thunman H, Leckner B. Mass transfer under segregation conditions in fluidized beds. Fuel 2017;195:105–12. https://doi.org/10.1016/j.fuel.2017.01.021.

[3] Lundberg L, Tchoffor PA, Pallarès D, Johansson R, Thunman H, Davidsson K. Influence of surrounding conditions and fuel size on the gasification rate of biomass char in a fluidized bed. Fuel Process Technol 2016;144:323–33. https://doi.org/10.1016/j.fuproc.2016.01.002.

[4] Olsson J, Pallarès D, Johnsson F. Lateral fuel dispersion in a large-scale bubbling fluidized bed. Chem Eng Sci 2012;74:148–59. https://doi.org/10.1016/j.ces.2012.02.027.

[5] Bellgardt D, Werther J. A novel method for the investigation of particle mixing in gas-solid systems. Powder Technol 1986;48:173–80. https://doi.org/10.1016/0032-5910(86)80076-6.

[6] Gómez-Barea A, Leckner B. Modeling of biomass gasification in fluidized bed. Prog Energy Combust Sci 2010;36(4):444–509. https://doi.org/10.1016/j.pecs.2009.12.002.

[7] Winaya INS, Shimizu T, Yamada D. A new method to evaluate horizontal solid dispersion in a bubbling fluidized bed. Powder Technol 2007;178:173–8. https://doi.org/10.1016/j.powtec.2007.05.005.

[8] Liu D, Chen X. Lateral solids dispersion coefficient in large-scale fluidized beds. Combust Flame 2010;157:2116–24. https://doi.org/10.1016/j.combustflame.2010.04.020.

[9] Garcia-Gutierrez LM, Soria-Verdugo A, Ruiz-Rivas U. Optimization of the feeding ports location in a fluidized bed combustor based on Monte Carlo simulations of fuel particles motion. Fuel 2015;141:82–92. https://doi.org/10.1016/j.fuel.2014.10.027.

[10] Niklasson F, Thunman H, Johnsson F, Leckner Bo. Estimation of Solids Mixing in a Fluidized-Bed Combustor. Ind Eng Chem Res 2002;41(18):4663–73. https://doi.org/10.1021/ie020173s.

[11] Rowe PN, Partridge BA, Cheney AG, Henwood GA, Lyall E. The mechanisms of solids mixing in fluidised beds. Chem Eng Res Des 1965;43a:271–86.

[12] Rowe PN, Nienow AW, Agbim AJ. The mechanisms by which particles segregate in gas fluidised beds - binary systems of near-spherical particles. Trans Inst Chem Eng 1972;50:310–23.

[13] Rowe PN, Nienow AW. Particle mixing and segregation in gas fluidised beds. A review. Powder Technol 1976;15(2):141–7. https://doi.org/10.1016/0032-5910(76)80042-3.

[14] Breault RW. A review of gas–solid dispersion and mass transfer coefficient correlations in circulating fluidized beds. Powder Technol 2006;163:9–17. https://doi.org/10.1016/j.powtec.2006.01.009.

[15] Chaouki J, Larachi F, Duduković MP. Noninvasive Tomographic and Velocimetric Monitoring of Multiphase Flows. Ind Eng Chem Res 1997;36(11):4476–503. https://doi.org/10.1021/ie970210t.

[16] Rios GM, Dang Tran K, Masson H. Free object motion in a gas fluidized bed. Chem Eng Commun 1986;47(4-6):247–72. https://doi.org/10.1080/00986448608911767.

[17] Lim KS, Agarwal PK. Circulatory motion of a large and lighter sphere in a bubbling fluidized bed of smaller and heavier particles. Chem Eng Sci 1994;49:421–4. https://doi.org/10.1016/0009-2509(94)87014-4.

[18] Pallarès D, Johnsson F. A novel technique for particle tracking in cold 2-dimensional fluidized beds—simulating fuel dispersion. Chem Eng Sci 2006;61(8):2710–20. https://doi.org/10.1016/j.ces.2005.11.030.

[19] Soria-Verdugo A, Garcia-Gutierrez LM, García-Hernando N, Ruiz-Rivas U. Buoyancy effects on objects moving in a bubbling fluidized bed. Chem Eng Sci 2011;66(12):2833–41. https://doi.org/10.1016/j.ces.2011.03.055.

[20] Soria-Verdugo A, Garcia-Gutierrez LM, Sanchez-Delgado S, Ruiz-Rivas U. Circulation of an object immersed in a bubbling fluidized bed. Chem Eng Sci 2011;66:78–87. https://doi.org/10.1016/j.ces.2010.10.006.

[21] Garcia-Gutierrez LM, Soria-Verdugo A, Garcia-Hernando N, Ruiz-Rivas U. Simulation of object motion in a bubbling fluidized bed using a Monte Carlo method. Chem Eng Sci 2013;96:26–32. https://doi.org/10.1016/j.ces.2013.02.067.

[22] Buist KA, van Erdewijk TW, Deen NG, Kuipers JAM. Determination and comparison of rotational velocity in a pseudo 2-D fluidized bed using magnetic particle tracking and discrete particle modeling. AIChE J 2015;61(10):3198–207. https://doi.org/10.1002/aic.v61.1010.1002/aic.14949.

[23] Moslemian D, Devanathan N, Dudukovic MP. Radioactive particle tracking technique for investigation of phase recirculation and turbulence in multiphase systems. Rev Sci Instrum 1992;63:4361–72. https://doi.org/10.1063/1.1143736.

[24] Weinell CE, Dam-Johansen K, Johnsson JE. Single-particle behaviour in circulating fluidized beds. Powder Technol 1997;92:241–52. https://doi.org/10.1016/S0032-5910(97)03245-2.

[25] Stein M, Ding YL, Seville JPK, Parker DJ. Solids motion in bubbling gas fluidised beds. Chem Eng Sci 2000;55:5291–300. https://doi.org/10.1016/S0009-2509(00)00177-9.

[26] Halow J, Holsopple K, Crawshaw B, Daw S, Finney C. Observed Mixing Behavior of Single Particles in a Bubbling Fluidized Bed of Higher-Density Particles. Ind Eng Chem Res 2012;51(44):14566–76. https://doi.org/10.1021/ie301517w.

[27] Fotovat F, Ansart R, Hemati M, Simonin O, Chaouki J. Sand-assisted fluidization of large cylindrical and spherical biomass particles: Experiments and simulation. Chem Eng Sci 2015;126:543–59. https://doi.org/10.1016/j.ces.2014.12.022.

[28] Fotovat F, Chaouki J. Characterization of the upward motion of an object immersed in a bubbling fluidized bed of fine particles. Chem Eng J 2015;280:26–35. https://doi.org/10.1016/j.cej.2015.05.130.

[29] Köhler A, Pallarès D, Johnsson F. Magnetic tracking of a fuel particle in a fluid-dynamically down-scaled fluidised bed. Fuel Process Technol 2017;162:147–56. https://doi.org/10.1016/j.fuproc.2017.03.018.

[30] Köhler A, Rasch A, Pallarès D, Johnsson F. Experimental characterization of axial fuel mixing in fluidized beds by magnetic particle tracking. Powder Technol 2017;316:492–9. https://doi.org/10.1016/j.powtec.2016.12.093.

[31] Schlichthaerle P, Werther J. Solids mixing in the bottom zone of a circulating fluidized bed. Powder Technol 2001;120:21–33. https://doi.org/10.1016/S0032-5910(01)00342-4.

[32] Qian X, Guoquan H, Mingjiang N, Kefa C, Tao T. Lateral Dispersion of Large Coal Particles in an Industrial-Scale Fluidised Bed Combustor. J Zhejiang Univ (Engineering Sci 1987;1:69–77.

[33] Sette E, Pallarès D, Johnsson F. Influence of bulk solids cross-flow on lateral mixing of fuel in dual fluidized beds. Fuel Process Technol 2015;140:245–51. https://doi.org/10.1016/j.fuproc.2015.09.017.

[34] Pallarès D, Díez PA, Johnsson F. Experimental Analysis of Fuel Mixing Patterns in a Fluidized Bed. 12th Int Conf Fluid - New Horizons Fluid Eng 2007.

[35] Nienow AW, Rowe PN, Chiwa T. Mixing and segregation of a small proportion of large particles in gas fluidized beds of considerably. AIChE Symp Ser 1978;74:45–53.

[36] Bilbao R, Lezaun J, Menéndez M, Abanades JC. Model of mixing—segregation for straw/sand mixtures in fluidized beds. Powder Technol 1988;56(3):149–55.

[37] Bilbao R, Lezaun J, Menéndez M, Izquierdo MT. Segregation of straw/sand mixtures in fluidized beds in non-steady state. Powder Technol 1991;68(1):31–5.

[38] Nguyen TH, Grace JR. Forces on objects immersed in fluidized beds. Powder Technol 1978;19:255–64. https://doi.org/10.1016/0032-5910(78)80034-5.

[39] Farzaneh M, Sasic S, Almstedt A-E, Johnsson F, Pallarès D. A study of fuel particle movement in fluidized beds. Ind Eng Chem Res 2013;52(16):5791–805. https://doi.org/10.1021/ie301515v.

[40] Hernández-Jiménez F, Garcia-Gutierrez LM, Soria-Verdugo A, Acosta-Iborra A. Fully coupled TFM-DEM simulations to study the motion of fuel particles in a fluidized bed. Chem Eng Sci 2015;134:57–66. https://doi.org/10.1016/j.ces.2015.04.028.

[41] Farzaneh M, Sasic S, Almstedt A-E, Johnsson F, Pallarès D. A novel multigrid technique for Lagrangian modeling of fuel mixing in fluidized beds. Chem Eng Sci 2011;66:5628–37. https://doi.org/10.1016/j.ces.2011.07.060.

[42] Davidson JF, Harrison D. Fluidised particles. Cambridge: Cambridge University Press; 1963.

[43] Grace JR, Harrison D. The behaviour of freely bubbling fluidised beds. Chem Eng Sci 1969;24(3):497–508. https://doi.org/10.1016/0009-2509(69)85021-9.

[44] Grace JR, Clift R. On the two-phase theory of fluidization. Chem Eng Sci 1974;29(2):327–34. https://doi.org/10.1016/0009-2509(74)80039-4.

[45] Werther J. Influence of the bed diameter on the hydrodynamics of gas fluidized beds. AIChE Symp Ser 1974;70:53–62.

[46] Johnsson F, Andersson S, Leckner B. Expansion of a freely bubbling fluidized bed. Powder Technol 1991;68(2):117–23. https://doi.org/10.1016/0032-5910(91)80118-3.

[47] Wiesendorf V, Hartge E-U, Werther J, Johnsson F, Sterneus J, Leckner B, et al. The CFB boiler in Gardanne - an experimental investigation of its bottom zone. In: Proc. 15th Int. Conf. Fluid. Bed Combust., New York; 1999. p. 151. https://doi.org/10.1016/s0140-6701(00)94625-3.

[48] Lyngfelt A, Mand L-E, Leckner B. Progress of combustion in the furnace of a circulating fluidized bed boiler. Symp Combust 1996;26:3253–9. https://doi.org/10.1016/S0082-0784(96)80171-8.

[49] Darton RC, La Nauze R, Davidson JF, Harrison D. Bubble Growth Due To Coalescence in Fluidized Beds. Trans Inst Chem Eng 1977;55:274–80.

[50] Kunii D, Levenspiel O. Fluidization Engineering. Stoneham, MA: Butterworth-Heinemann; 1991.

[51] Köhler A, Pallarès D, Johnsson F. Modeling Axial Mixing of Fuel Particles in the Dense Region of a Fluidized Bed. Energy Fuels 2020;34(3):3294–304. https://doi.org/10.1021/acs.energyfuels.9b04194.

[52] Karri SBR, Werther J. Gas distributor and plenum design in fluidized beds. In: Yang W-C, editor. Handb. Fluid. fluid-particle Syst., Marcel Dekker Inc.; 2003, p. 164–79.

[53] Whitehead AB. Some problems in large-scale fluidized beds. In: Davidson JF, Harrison D, editors. Fluidization. London: Academic Press; 1971. p. 781–811.

[54] Chhabra RP. Bubbles, Drops, and Particles in Non-Newtonian Fluids. Boca Raton, FL: CRC Press; 2007. https://doi.org/https://doi.org/10.1201/9781420015386.
[55] Rees AC, Davidson JF, Dennis JS, Hayhurst AN. The rise of a buoyant sphere in a gas-fluidized bed. Chem Eng Sci 2005;60:1143–53. https://doi.org/10.1016/j.ces.2004.09.045.
[56] Garcia-Gutierrez LM, Soria-Verdugo A, Marugán-Cruz C, Ruiz-Rivas U. Simulation and experimental study on the motion of non-reacting objects in the freeboard of a fluidized bed. Powder Technol 2014;263:112–20. https://doi.org/10.1016/j.powtec.2014.04.085.
[57] Einstein A. Investigations on the theory of the Brownian movement. Dover; 1956.
[58] Mostoufi N, Chaouki J. Local solid mixing in gas–solid fluidized beds. Powder Technol 2001;114:23–31. https://doi.org/10.1016/S0032-5910(00)00258-8.
[59] Sette E, Pallarès D, Johnsson F. Experimental quantification of lateral mixing of fuels in fluid-dynamically down-scaled bubbling fluidized beds. Appl Energy 2014;136:671–81. https://doi.org/10.1016/j.apenergy.2014.09.075.